THE EUROPEAN
PHYSICAL JOURNAL B

Regular Article - Solid State and Materials

Bound states for massive Dirac fermions in graphene in a magnetic step field

L. Dell'Anna[1,a] , A. Alidoust Ghatar[2], and D. Jahani[2]

[1] Dipartimento di Fisica e Astronomia, University of Padova, via F. Marzolo 8, 35151 Padua, Italy
[2] Material and Energy Research Center, Tehran, Iran

Abstract. We calculate the spectrum of massive Dirac fermions in graphene in the presence of an inhomogeneous magnetic field modeled by a step function. We find an analytical universal relation between the bandwidths and the propagating velocities of the modes at the border of the magnetic region, showing how, by tuning the mass term, one can control the speed of these traveling edge states.

1 Introduction

Graphene is generally described by massless Dirac fermions [1], nevertheless different techniques have been developed for nanotechnological applications and for exploring non-trivial topological properties, to generate a gap at the Dirac points [2–4] so to include a mass term in the Dirac–Weyl Hamiltonian, which describes the low-energy physics in graphene [1,5–7]. Mass terms, confining scalar potentials or magnetic fields can spoil the simple linear dispersion of the original massless Dirac fermions [8–15].

In particular, applying inhomogeneous magnetic fields perpendicularly to the graphene sheet one can produce bound states trapped in the vicinity of the discontinuity of the magnetic field and propagating along the magnetic edges [16–19]. Several bound state spectra have been already obtained and scattering problems solved for massless Dirac fermions in graphene embedded in discontinuous magnetic fields employing boundary conditions [16–31].

What we are going to present in this work, instead, is the bound state spectrum for massive Dirac fermions in the simplest inhomogeneous magnetic pattern described by a step function, which provides a prime example of interface between magnetic and non-magnetic regions.

We see that edge states emerge at threshold values of a longitudinal momentum, and upon increasing its absolute value, they rapidly approach the relativistic bulk Landau levels. In the massless limit we recover the known results [16,18]. We observe some universal behaviors, in particular we show analytically that, in this magnetic structure, for each band, the bound state threshold does not depend on the mass term even if the energy levels do depend on it. Moreover we show that the maximum of the velocity of the edge modes

[a] e-mail: luca.dellanna@unipd.it (corresponding author)

propagating along the magnetic boundary, as a function of the mass term, seems to be proportional to the bandwidth; therefore, the ratio between the bandwidth and the corresponding maximum velocity is a mass-independent quantity.

Our findings can be also verified experimentally. Actually, it has been observed that a band gap of about 30 meV can be obtained placing several layers of hexagonal boron nitride in contact with graphene [32], or even in a more tunable setup, by exploiting strain-induced band-structure engineering, an energy-gap value from zero up to 0.9 eV can be obtained by share deformations of the monolayer graphene [33]. Finally, a magnetic step can be easily generated by placing a ferromagnetic material on top of graphene.

In summary, by this analysis, we show how, by tuning the mass term, feasible experimentally, one can control the propagating speed of the modes located at the edge of a magnetic region, relevant for future tunable graphene-based mesoscopic devices.

2 Magnetic step

Let us consider a magnetic field perpendicular to the plane of graphene, z-direction, and with a step profile along one direction in the plane of graphene, $B_z(x) = B \, \theta(x)$, where $\theta(x)$ is the Heaviside theta function. The potential vector is, therefore, $\mathbf{A} = (0, A(x), 0)$, defined by

$$A(x) = \frac{\hbar c}{e l_B^2} x \, \theta(x), \qquad (2.1)$$

where $\hbar = h/2\pi$ with h the Planck constant, c the speed of light, e the elementary charge, and $l_B = \sqrt{\hbar c/eB}$ the magnetic length. We are supposing that the length scale over which $B(x)$ significantly varies, say λ_B, is

assumed much larger than the lattice spacing so that, at low energy scales, the two Dirac points in the massless limit are not coupled by the magnetic field and can be treated separately. We assume also that λ_B is much smaller than the quasiparticle Fermi wavelength so that we can safely approximate $B(x)$ as a step function. The massive Dirac–Weyl equation is then given by

$$\Big(v_F(\sigma_x \pi_x + \sigma_y \pi_y) + \Delta \sigma_z \Big)\psi(x,y) = \varepsilon \psi(x,y), \quad (2.2)$$

with v_F the Fermi velocity, $\sigma_x, \sigma_y, \sigma_z$ the Pauli matrices, π the momentum operator $\boldsymbol{\pi} = -i\hbar \boldsymbol{\nabla} + \frac{e}{c}\mathbf{A}$ and Δ the energy gap. Because of the translational invariance along the y-direction, the spinor can be written as

$$\psi(x,y) = e^{ik_y y}\,\psi(x) \equiv e^{ik_y y}\begin{pmatrix} a(x) \\ b(x). \end{pmatrix} \quad (2.3)$$

Let us split the space in two regions, I and II.

Region I. For $x > 0$, from Eq. (2.2), we can write the following equations for the two components

$$\Delta\, a(x) - iv_F\left[\hbar\frac{d}{dx} + \left(\hbar k_y + \frac{eA(x)}{c}\right)\right]b(x) = \varepsilon\, a(x) \quad (2.4)$$

$$-iv_F\left[\hbar\frac{d}{dx} - \left(\hbar k_y + \frac{eA(x)}{c}\right)\right]a(x) - \Delta\, b(x) = \varepsilon\, b(x). \quad (2.5)$$

From these equations, putting one into the other, we obtain

$$\left[l_B^2\hbar^2\frac{d^2}{dx^2} - \left(\hbar k_y l_B + \left(\frac{el_B}{c}\right)A(x)\right)^2 \right.$$
$$\left. - \left(\frac{l_B^2 e}{c}\right)\left(\frac{dA(x)}{dx}\right) + \frac{l_B^2}{v_F^2}(\varepsilon^2 - \Delta^2)\right]a(x) = 0. \quad (2.6)$$

Using Eq. (2.1), we can write the following equation, for $x > 0$,

$$\left[\frac{d^2}{d\left(\frac{x}{l_B}\right)^2} - (k_y l_B + x/l_B)^2 - 1 + \frac{l_B^2}{\hbar^2 v_F^2}(\varepsilon^2 - \Delta^2)\right]$$
$$a(x) = 0. \quad (2.7)$$

Notice that this is an effective one-dimensional Schrödinger equation where, for $k_y < 0$, the potential develops a minimum within the magnetic region for which bound state solutions exist, with energies such that $|k_y| > \sqrt{(\varepsilon^2 - \Delta^2)}/\hbar v_F$, as we will verify in what follows. Making the following change of variables:

$$\xi = k_y l_B + x/l_B, \quad (2.8)$$

Eq. (2.7) becomes simply

$$\left(\frac{d^2}{d\xi^2} - \xi^2 - 1 + 2\eta\right)a(x) = 0, \quad (2.9)$$

where we defined the quantity, which is generally a real number,

$$\eta = \frac{l_B^2}{2\hbar^2 v_F^2}(\varepsilon^2 - \Delta^2). \quad (2.10)$$

The normalizable solution of Eq. (2.9) is

$$a(x) = c_I\, D_{\eta-1}(\sqrt{2}\,\xi), \quad (2.11)$$

where $D_\eta(z)$ is a parabolic cylinder function and c_I a constant value. Notice that if $\eta = n$ is a non-negative integer number, one can write $D_n(\sqrt{2}\xi) = 2^{-n/2}e^{-\xi^2/2}H_n(\xi)$, namely in terms of the Hermite polynomials $H_n(\xi) = (-1)^n e^{\xi^2}\frac{d^n}{d\xi^n}e^{-\xi^2}$. To find the second component of the spinor we can write

$$(\varepsilon + \Delta)b(x) = -i\frac{\hbar v_F}{l_B}\left(\frac{d}{d\xi} - \xi\right)a(x), \quad (2.12)$$

and using the recursive relation

$$\frac{d}{dz}D_{\eta-1}(z) - \frac{z}{2}D_{\eta-1}(z) + D_\eta(z) = 0 \quad (2.13)$$

we get the complete spinorial wavefunction

$$\psi(x) = c_I\begin{pmatrix} D_{\eta-1}(\sqrt{2}\,\xi) \\ \frac{i\sqrt{2}\,\hbar v_F}{(\varepsilon+\Delta)l_B}D_\eta(\sqrt{2}\,\xi) \end{pmatrix}. \quad (2.14)$$

Region II. For $x < 0$, we obtain the following equation by placing $A(x) = 0$ in Eqs. (2.4), (2.5)

$$\frac{(\varepsilon - \Delta)}{\hbar v_F}a(x) + i\left(\frac{d}{dx} + k_y\right)b(x) = 0 \quad (2.15)$$

$$\frac{(\varepsilon + \Delta)}{\hbar v_F}b(x) + i\left(\frac{d}{dx} - k_y\right)a(x) = 0 \quad (2.16)$$

so that, analogously to what done in the other case, we can write

$$\left[\frac{d^2}{dx^2} - k_y^2 + \frac{(\varepsilon^2 - \Delta^2)}{\hbar^2 v_F^2}\right]a(x) = 0 \quad (2.17)$$

whose solution can be written as

$$a(x) = c_{II}\left(e^{k_x x} + r\, e^{-k_x x}\right) \quad (2.18)$$

with c_{II} and r constant values and where we defined

$$k_x = \sqrt{k_y^2 - (\varepsilon^2 - \Delta^2)/\hbar^2 v_F^2}. \quad (2.19)$$

The bound state solutions are those with $k_y^2 > \left(\varepsilon^2 - \Delta^2\right)/\hbar^2 v_F^2$ so that, for $x < 0$, the only normalizable contribution in Eq. (2.18) is the first one, $a(x) = c_{\mathrm{II}} e^{k_x x}$. Using Eq. (2.16) we get the other component of the spinor, $b(x) = -i\frac{\hbar v_F}{(\varepsilon+\Delta)}\left(\frac{\mathrm{d}}{\mathrm{d}x} - k_y\right) a(x)$, getting the following bound-state wavefunction

$$\psi(x) = c_{\mathrm{II}}\, e^{k_x x} \begin{pmatrix} 1 \\ \frac{i\hbar v_F(k_y - k_x)}{(\varepsilon+\Delta)} \end{pmatrix}. \qquad (2.20)$$

Imposing the matching condition at $x = 0$, from Eqs. (2.14) and (2.20) we find

$$l_B\,(k_y - k_x)\, D_{(\varepsilon^2 l_B^2 - \Delta^2 l_B^2)/(2\hbar^2 v_F^2)-1}(\sqrt{2}\,k_y l_B)$$
$$= \sqrt{2}\, D_{(\varepsilon^2 l_B^2 - \Delta^2 l_B^2)/(2\hbar^2 v_F^2)}\,(\sqrt{2}\,k_y l_B), \qquad (2.21)$$

where we used Eq. (2.10) and where k_x is defined in Eq. (2.19).

If we put $\Delta = 0$ in Eq. (2.21), the matching condition reduces to that of the gapless graphene [16]. In this case in addition to the finite-energy states, solution of the above equation, there is also the zero energy state, $\tilde{\epsilon}_0 = 0$, for $k_y < 0$, whose wavefunction is

$$\psi_0(x) = \begin{pmatrix} 0 \\ 1 \end{pmatrix} \left(\theta(-x) + \theta(x)e^{-x^2/2}\right) e^{-k_y x}. \qquad (2.22)$$

To find the finite-energy spectrum defined by Eq. (2.21), in the general case of gapped graphene, it is convenient to introduce the dimensionless parameters

$$\tilde{\epsilon}^2 = (\varepsilon^2 l_B^2)/(v_F^2 \hbar^2), \qquad (2.23)$$
$$\tilde{\Delta}^2 = (\Delta^2 l_B^2)/(v_F^2 \hbar^2), \qquad (2.24)$$
$$\tilde{k}_y = k_y l_B, \qquad (2.25)$$

such that Eq. (2.21) can be written as it follows:

$$\left(\tilde{k}_y - \sqrt{\tilde{k}_y^2 - (\tilde{\epsilon}^2 - \tilde{\Delta}^2)}\right) D_{(\tilde{\epsilon}^2 - \tilde{\Delta}^2)/2-1}(\sqrt{2}\,\tilde{k}_y)$$
$$= \sqrt{2}\, D_{(\tilde{\epsilon}^2 - \tilde{\Delta}^2)/2}(\sqrt{2}\,\tilde{k}_y), \qquad (2.26)$$

whose solutions are quantized, $\tilde{\epsilon}_n$, with $n = 1, 2, 3, \dots$. Notice that Eq. (2.26) is valid for $\tilde{\epsilon} \neq -\tilde{\Delta}$. Also in this case there is an extra-state with a completely flat band at $\tilde{\epsilon}_0 = -\tilde{\Delta}$ whose wavefunctions is described by Eq. (2.22), localized at the edge, where the discontinuity of the magnetic field is located, but whose band is not dispersive.

3 Results

The dispersive energy levels are obtained by solving the matching condition Eq. (2.26). We verified that the

bound states exist for $k_y < 0$ and for

$$\tilde{\epsilon}^2 \leq \tilde{k}_y^2 + \tilde{\Delta}^2, \qquad (3.27)$$

as shown in Fig. 1. For $k_y \to -\infty$ the energies $\tilde{\epsilon}_n$, solutions of Eq. (2.26), approach the Landau levels for relativistic massive particles

$$\tilde{E}_n = \pm\sqrt{\tilde{\Delta}^2 + 2n} \qquad (3.28)$$

with n positive integer numbers. In this limit the wavefunctions are written in terms of Hermite polynomials, as already mentioned.

For any n, $\tilde{E}_n$ is the maximum value of $\tilde{\epsilon}_n$. The minimum value of $\tilde{\epsilon}_n$ is located at the threshold, $\tilde{k}_y = p_n \equiv -\sqrt{\tilde{\epsilon}_n^2 - \tilde{\Delta}^2}$, solution of the following equation:

$$p_n D_{p_n^2/2-1}(\sqrt{2}\,p_n) - \sqrt{2}\,D_{p_n^2/2}(\sqrt{2}\,p_n) = 0; \qquad (3.29)$$

therefore p_n does not depend on the mass term, as shown in Fig. 2 (first two plots).

For instance, numerically, we get $p_1 \approx -1.31325$, $p_2 \approx -1.92427$, $p_3 \approx -2.38626$ and so on. We have then

$$\min\left[\tilde{\epsilon}_n(\tilde{k}_y)\right] = \tilde{\epsilon}_n(p_n) = \sqrt{\tilde{\Delta}^2 + p_n^2}, \qquad (3.30)$$

see Fig. 3 (first plot) where these quantities are reported as functions of the mass term $\tilde{\Delta}$. These bands are dispersive and the corresponding bandwidths can be easily calculated

$$\delta\tilde{\epsilon}_n = \tilde{E}_n - \tilde{\epsilon}_n(p_n) = \sqrt{\tilde{\Delta}^2 + 2n} - \sqrt{\tilde{\Delta}^2 + p_n^2}. \qquad (3.31)$$

In Fig. 3 (second plot), the bandwidths of the first three levels as functions of the mass $\tilde{\Delta}$ are reported. The wavefunctions associated to the dispersive part of the band $\tilde{\epsilon}_n$ are states localized at the edge of the magnetic field. These edge states provide one-dimensional channels freely propagating along the magnetic boundary. Indeed, we can define the following velocities:

$$\tilde{v}_n(\tilde{k}_y) = \frac{d\tilde{\epsilon}_n}{d\tilde{k}_y}, \qquad (3.32)$$

and observe that their maximum absolute values are reached right at the threshold

$$\max\left|\tilde{v}_n(\tilde{k}_y)\right| = \left|\tilde{v}_n(p_n)\right| \qquad (3.33)$$

while for modes with $|k_y| > |p_n|$, $|\tilde{v}_n(\tilde{k}_y)|$ are smaller, see Fig. 2 (last plot) for $n = 1, 2$. In particular, for $\tilde{\Delta} = 0$ we have $|\tilde{v}_n(p_n)| = 1$, while increasing the mass term the modulus of the velocity decreases. Surprisingly we find that the ratios between the bandwidths and the maximum velocities, although both functions of the
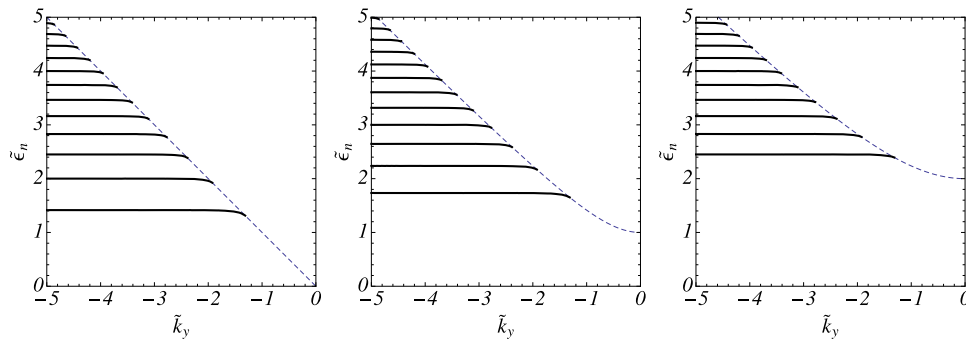
Fig. 1 Spectrum of the low-lying positive-energy edge states at a magnetic step for $\tilde{\Delta} = 0$ (left), $\tilde{\Delta} = 1$ (middle) and $\tilde{\Delta} = 2$ (right). The dashed line denotes the threshold value for edge state solutions, $\tilde{\epsilon} = \sqrt{\tilde{k}_y^2 + \tilde{\Delta}^2}$. For large negative $\tilde{k}_y$ the levels rapidly approach the Landau level values $\sqrt{\tilde{\Delta}^2 + 2n}$, with $n \geq 1$ positive integer numbers. The negative-energy spectrum is specular with, in addition, the flat zeroth energy level $\tilde{\epsilon}_0 = -\tilde{\Delta}$
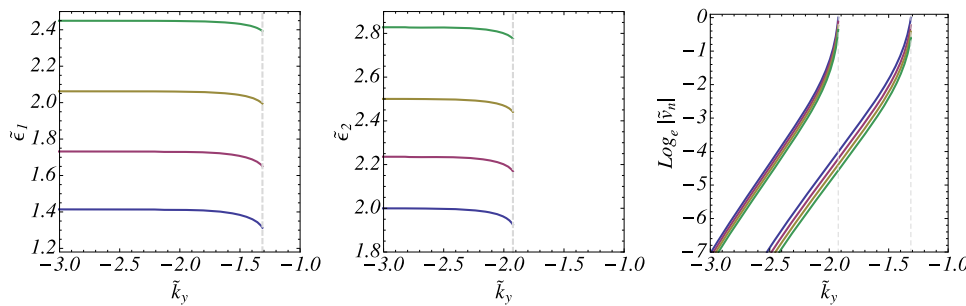
Fig. 2 First energy level $\tilde{\epsilon}_1$ (left) and second energy level $\tilde{\epsilon}_2$ (middle), solutions of Eq. (2.26), for increasing values of the mass term, $\tilde{\Delta} = 0$ (blue line), $\tilde{\Delta} = 1$ (red line), $\tilde{\Delta} = 1.5$ (yellow line), $\tilde{\Delta} = 2$ (green line). (Right) Modulus of the velocities, in log-scale, associated to the first and the second energy levels, defined as $\tilde{v}_n = \partial_{\tilde{k}_y} \tilde{\epsilon}_n$, for the same values of $\tilde{\Delta}$ as in the first two plots, $\tilde{\Delta} = 0, 1, 1.5, 2$
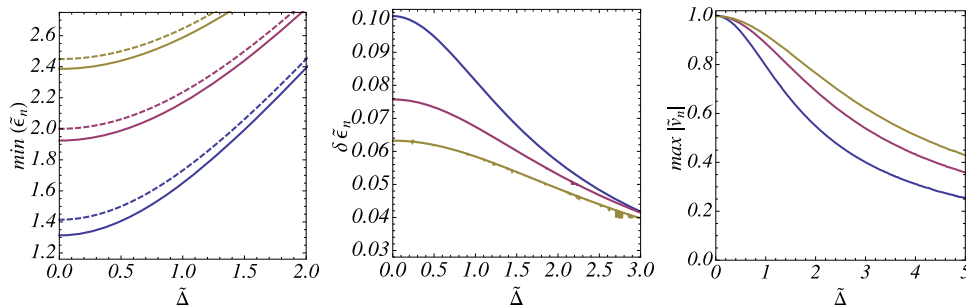

Fig. 3 (Left) Minima of the first three energy levels $\tilde{\epsilon}_n(k_y)$, with $n = 1$ (blue solid line), $n = 2$ (red solid line), $n = 3$ (yellow solid line), associated to the edge modes with $k_y = p_n$, as functions of the mass term (solid lines). The dashed lines are the corresponding energy levels in the deep bulk embedded by a uniform magnetic field, described by the Landau levels $\tilde{E}_n = \sqrt{\tilde{\Delta}^2 + 2n}$. (Middle) Bandwidths of the first three levels, defined as the difference between the Landau levels, at the bulk, and the energy at the boundary, $\delta\tilde{\epsilon}_n = \tilde{E}_n - \min(\tilde{\epsilon}_n)$. (Right) Maximum velocities obtained at the threshold of the three levels, see Fig. 2, as functions of the mass term. In all the plots, the blue lines correspond to $n = 1$, the red lines to $n = 2$, the yellow lines to $n = 3$

mass term, are universal quantities, namely, in their turn, the ratios do not depend on the mass, but are equal to the bandwidths in the massless case, namely at $\tilde{\Delta} = 0$. Actually we observe numerically, at least for the first three levels reported in Fig. 3, that

$$\frac{\delta\tilde{\epsilon}_n[\tilde{\Delta}]}{\delta\tilde{\epsilon}_n[0]} = |\tilde{v}_n(p_n)|[\tilde{\Delta}]. \tag{3.34}$$

We checked that the curves in the second and third plots of Fig. 3 perfectly overlaps after rescaling according to Eq. (3.34). This observation allows us to explic-

itly write the highest velocities as analytical functions of the mass parameter $\tilde{\Delta}$

$$|\tilde{v}_n(p_n)| = \frac{1}{\sqrt{2n} - |p_n|} \left(\sqrt{\tilde{\Delta}^2 + 2n} - \sqrt{\tilde{\Delta}^2 + p_n^2} \right),$$
(3.35)

with p_n solution of Eq. (3.29). We finally notice that all curves representing $\tilde{v}_n(\tilde{k}_y)$ in log-scale reported in the last plot of Fig. 3 collapse into a single curve after a rescaling, $\tilde{v}_n(\tilde{k}_y)[\tilde{\Delta}] = \tilde{v}_n(\tilde{k}_y)[0]|\tilde{v}_n(p_n)|[\tilde{\Delta}]$. Calling, for each band, $\tilde{v}_n^o(\tilde{k}_y) \equiv \tilde{v}_n(\tilde{k}_y)[\tilde{\Delta} = 0]$ the velocity in the massless case, we have the following simple scaling law for the velocities in the presence of a gap

$$\tilde{v}_n(\tilde{k}_y) = \frac{\tilde{v}_n^o(\tilde{k}_y)}{\sqrt{2n} - |p_n|} \left(\sqrt{\tilde{\Delta}^2 + 2n} - \sqrt{\tilde{\Delta}^2 + p_n^2} \right).$$
(3.36)

4 Conclusion

In this paper we derived the bound state spectrum for massive Dirac fermions in graphene subjected to a perpendicular magnetic field with a step function profile. We showed that the energy levels approach the relativistic Landau levels while the dispersive parts of the bands exhibit some universal behaviors. We find that the mass term modifies the bulk spectrum while reducing the number and the speed of the traveling modes at the border of the magnetic region, however the threshold of each bound states does not depends on the mass term and the ratio between the maximum propagating velocities and the bandwidths is also a mass-independent quantity. In conclusion, we show how, by tuning the mass term, one can control the speed of the edge modes traveling along the boundary of the magnetic region, paving the way for novel tunable graphene-based mesoscopic devices.

Author contributions

All authors contributed to the writing of the paper, agreed on the approach to pursue and performed the calculations. LD and DJ conceived the work, LD drew the results.

Data Availability Statement This manuscript has no associated data or the data will not be deposited. [Authors' comment: The datasets generated during and/or analysed during the current study are available from the corresponding author on reasonable request.]

References

1. A.H. Castro Neto, F. Guinea, N.M.R. Peres, K.S. Novoselov, A.K. Geim, Rev. Mod. Phys. **81**, 109 (2009)
2. G.W. Semenoff, Phys. Rev. Lett. **53**, 2449 (1984)
3. F.D.M. Haldane, Phys. Rev. Lett. **61**, 2015 (1988)
4. C.L. Kane, E.J. Mele, Phys. Rev. Lett. **95**, 226801 (2005)
5. N.M.R. Peres, A.H. Castro Neto, F. Guinea, Phys. Rev. B **73**, 241403(R) (2006)
6. N.M.R. Peres, E.V. Castro, J. Phys. Condens. Matter **19**, 406231 (2007)
7. M. Farjam, H. Rafii-Tabar, Phys. Rev. B **79**, 045417 (2009)
8. S. Kuru, J. Negro, L.M. Nieto, J. Phys. Condens. Matter **21**, 455305 (2009)
9. C.G. Beneventano, E.M. Santangelo, J. Phys. A Math. Theor. **39**, 7457 (2006)
10. G. Giovannetti, P.A. Khomyakov, G. Brocks, P.J. Kelly, J. van den Brink, Phys. Rev. B **76**, 073103 (2007)
11. V.P. Gusynin, S.G. Sharapov, Phys. Rev. Lett. **95**, 146801 (2005)
12. M.O. Goerbig, Rev. Mod. Phys. **83**, 1193 (2011)
13. B. Midya, D.J. Fernndez, J. Phys. A Math. Theor. **47**(28), 285302 (2014)
14. J.M. Pereira Jr., V. Mlinar, F.M. Peeters, P. Vasilopoulos, Phys. Rev. B **74**, 045424 (2006)
15. M.R. Setare, D. Jahani, Phys. B **405**, 1433 (2010)
16. A. De Martino, L. Dell'Anna, R. Egger, Solid State Commun. **144**, 547 (2007)
17. T.K. Ghosh, A. De Martino, W. Häusler, L. Dell'Anna, R. Egger, Phys. Rev. B. **77**, 081404(R) (2008)
18. M.R. Masir, P. Vasilopoulos, A. Matulis, F.M. Peeters, Phys. Rev. B. **77**, 235443 (2008)
19. A. Kormanyos, P. Rakyta, L. Oroszlany, J. Cserti, Phys. Rev. B **78**, 045430 (2008)
20. A. De Martino, L. Dell'Anna, R. Egger, Phys. Rev. Lett. **98**, 066802 (2007)
21. M.R. Masir, P. Vasilopoulos, F.M. Peeters, New J. Phys. **11**, 095009 (2009)
22. N. Myoung, G. Ihm, S.J. Lee, Phys. E Low-Dimens. Syst. Nanostruct. **42**(10), 2808 (2010)
23. E.B. Choubabi, M.E. Bouziani, A. Jellal, Int. J. Geom. Meth. Mod. Phys. **7**, 909 (2010)
24. E. Milpas, M. Torres, G. Murguia, J. Phys. Condens. Matter **23**, 245304 (2011)

25. L. Dell'Anna, A. De Martino, Phys. Rev. B **79**, 045420 (2009)
26. S. Park, H.S. Sim, Phys. Rev. B **77**, 075433 (2008)
27. M.R. Masir, P. Vasilopoulos, F.M. Peeters, Appl. Phys. Lett. **93**, 242103 (2008)
28. S. Ghosh, M. Sharma, J. Phys. Condens. Matter **21**, 292204 (2009)
29. N. Myoung, G. Ihm, Phys. E **42**, 70 (2009)
30. N. Agrawal, S. Chosh, M. Sharma, I. J. Mod. Phys. B **27**, 1341003 (2013)
31. M. Esmailpour, Phys. B **534**, 150 (2018)
32. M.S. Fuhrer, Science **340**, 1414 (2013)
33. G. Cocco, E. Cadelano, L. Colombo, Phys. Rev. B **81**, 241412(R) (2010)